Mon. Not. R. astr. Soc. (1987) **224,** 75–91

The optical spectra of central galaxies in southern clusters: evidence for star formation

R. M. Johnstone and A. C. Fabian *Institute of Astronomy, Madingley Road, Cambridge CB3 0HA*

P. E. J. Nulsen *Mount Stromlo & Siding Spring Observatories, Private Bag, Woden PO, ACT 2606, Australia*

Accepted 1986 July 14. Received 1986 July 9; in original form 1986 May 13

Summary. We have observed 21 elliptical galaxies, of which nine are at the centre of clusters with cooling flows, and find that 12 have extended optical line emission. The spectra show line ratios indicating low ionization and are qualitatively similar to those observed in other cooling flows. A problem with the production of the large observed line luminosities is highlighted and explained by some ongoing star formation with the initial mass function of a disc galaxy. The rate of such star formation is as high as $100\,M_{\odot}\,\mathrm{yr}^{-1}$ in the case of PKS 0745−191, and in all the galaxies there is quantitative agreement between the Hβ line flux and the 4000-Å break measured from our blue spectra. Most of the gas (more than 90 per cent) must cool from X-ray temperatures and form low-mass objects without producing any detectable optical line radiation or hot young stars.

1 Introduction

It is now well established that groups and clusters of galaxies are luminous X-ray sources. Stewart *et al.* (1984) have demonstrated that in about 30 per cent of the systems studied the cooling time t_{cool} for the gas in the core of the cluster is less than the Hubble time H_0^{-1} and that this leads to a cooling flow on to the central galaxy. Typical mass flow rates are tens or hundreds of solar masses per year, while the most extreme example PKS 0745−191 (Fabian *et al.* 1985) has a flow rate of about $1000\,M_{\odot}\,\mathrm{yr}^{-1}$. As gas cools from about 10^6 to 10^4 K it emits in optical recombination and forbidden lines and might thereby be detected by ground-based telescopes. The gas cools further to temperatures where it presumably forms low-mass stars (for a review see Fabian, Nulsen & Canizares 1984).

While the primary evidence for the existence of a cooling flow is derived from the X-ray data, it is clear that in order to study the evolution of the cooling gas optical and infrared observations are required. Several optical studies of central galaxies in clusters have already been published (e.g. Cowie *et al.* 1983; Hu, Cowie & Wang 1985), but these workers have concentrated on the

yellow-red part of the spectrum which, although rich in emission lines, is relatively insensitive to the underlying stellar population.

In this paper we present flux-calibrated blue spectra covering the region from [O II] to [O III] and uncalibrated red spectra covering the region from [O I] to [S II]. With these data we study the relation of the emitting gas to the underlying stellar population and the relationship of these quantities to the larger-scale properties of the cooling flow.

2 The data

2.1 INSTRUMENTAL SET-UP

The observations presented here were obtained during 1983 June 10–13 at the Anglo–Australian Telescope (AAT) and are listed in Table 1. The RGO spectrograph was used with the IPCS at the focus of the 25-cm camera to obtain spectra with 2 Å resolution in the blue-yellow and 0.75 Å resolution in the red. Each pixel in the spatial direction corresponded to 2.2 arcsec, giving a total slit length of about 2 arcmin. The slit width for the blue spectra was 1.5 arcsec, except in the case of A1795 for which it was 2.0 arcsec. Most of the objects observed were central cluster galaxies, selected on the basis of known or suspected cooling flows or radio emission [generally present in cooling flows (Jones & Forman 1984)]. A few elliptical galaxies were observed as controls.

2.2 CALIBRATION

The spectra were wavelength calibrated using standard procedures available in the STARLINK spectral data reduction package SPICA from exposures of the Cu–Ar hollow cathode lamp taken between most object spectra. Before flux calibration and sky subtraction the data were corrected for the difference in response along the slit from a long observation of the sky. We interpolated across the spectrum of a star which was also contained in this frame.

The blue spectra (of which some examples are shown in Fig. 1) were flux calibrated using a wide-slit observation of the white dwarf standard star L970–30 (Oke 1974) after correction for atmospheric extinction using a standard extinction law for the AAT site. Finally, the blue spectra were corrected for interstellar galactic extinction on the basis of the $N_{\rm H\,I}$ column density measurements in the direction of the cluster (Stark *et al.*, in preparation). The transformation from $N_{\rm H\,I}$ to $E(B-V)$ was made using the relation (Bohlin, Savage & Drake 1978)

$$E(B-V)=2.08\times10^{-22}N_{\rm H\,I}$$

and a value of $R=3.1$ for the ratio of total to selective absorption. Seaton's (1979) extinction law was used.

There are two shortcomings of the data which render the flux calibration less accurate in some objects. First, the spectra were not always obtained with the slit oriented at the parallactic angle (see e.g. Filippenko 1982) since it was often aligned in the direction of 'blobs' seen close to the galaxy on the UK Schmidt Telescope sky survey. The second deficiency in the flux calibration is that the grating angle in the observation of the standard was such that no data were recorded shortward of 3855 Å. The flux calibration has therefore been quadratically extrapolated shortward of this wavelength. This will affect the flux in [O II] for galaxies with redshifts of less than $z=0.034$.

The night on which the red spectra were obtained was not photometric, and no flux calibration of these data has been attempted.

Table 1. Log of observations, with measured velocities and distances.

Object	Spectral Region	Integration Time (s)	Position Angle	Velocity km s^{-1}	Distance (Mpc)
PKS0745-191	Blue	1500	55	29050[1]	581
	Blue	1500	145		
	Red	1350	55		
A1060	Blue	1500	145	3611	72
NGC4261	Blue	1500	145	2120	42
NGC4696	Blue[2]	1500	85	2730	55
	Red[3]	2242	167		
NGC4760	Blue	1500	145	4346	87
IC4296	Blue	502	85	3692	74
PKS1404-267	Blue	1500	110	6283	126
	Blue	1500	200		
	Red	1459	110		
A1991	Blue	1500	127	17387	348
A2029	Blue	1500	100	22440	449
MKW3s	Blue	1500	100	12990	260
A1795	Red	1500	160	18293	366
Ophiuchus	Red	1500	135		
IC4765	Blue	1500	200	4315	86
SC2008-566	Red	1500	135		
NGC6876	Blue	900	258	3689	74
2028-566	Red	1500	183		
2103-45	Blue	75	100	8692	174
2215-359	Blue	600	17	34536	691
NGC7385	Blue	1300	17	7949	159
Sersic 159	Blue	1500	65	16398	328
	Blue	1500	0		
	Red	1500	240		
NGC7626	Blue	300	17	3599	72
A2626	Blue	600	17	16390	328
A2657	Red	1069	272		
A2670	Blue	500	17	22323	446
	Red	1500	240		
A85	Blue	589	17	18145	325
	Red	999	156		

[1] Redshift from Fabian *et al.* (1985).

The spectra were all taken with the slit centred on the galaxy except for the exposure on NGC 4696 where the slit positions were as follows.

[2] Slit 5 arcsec south of the nucleus.

[3] Slit 3 arcsec west of the nucleus.

Velocities are mean values where more than one blue spectrum was obtained. They are corrected to the frame of reference defined by the Local Group. H_0=50 km s^{-1} Mpc^{-1} is adopted throughout.

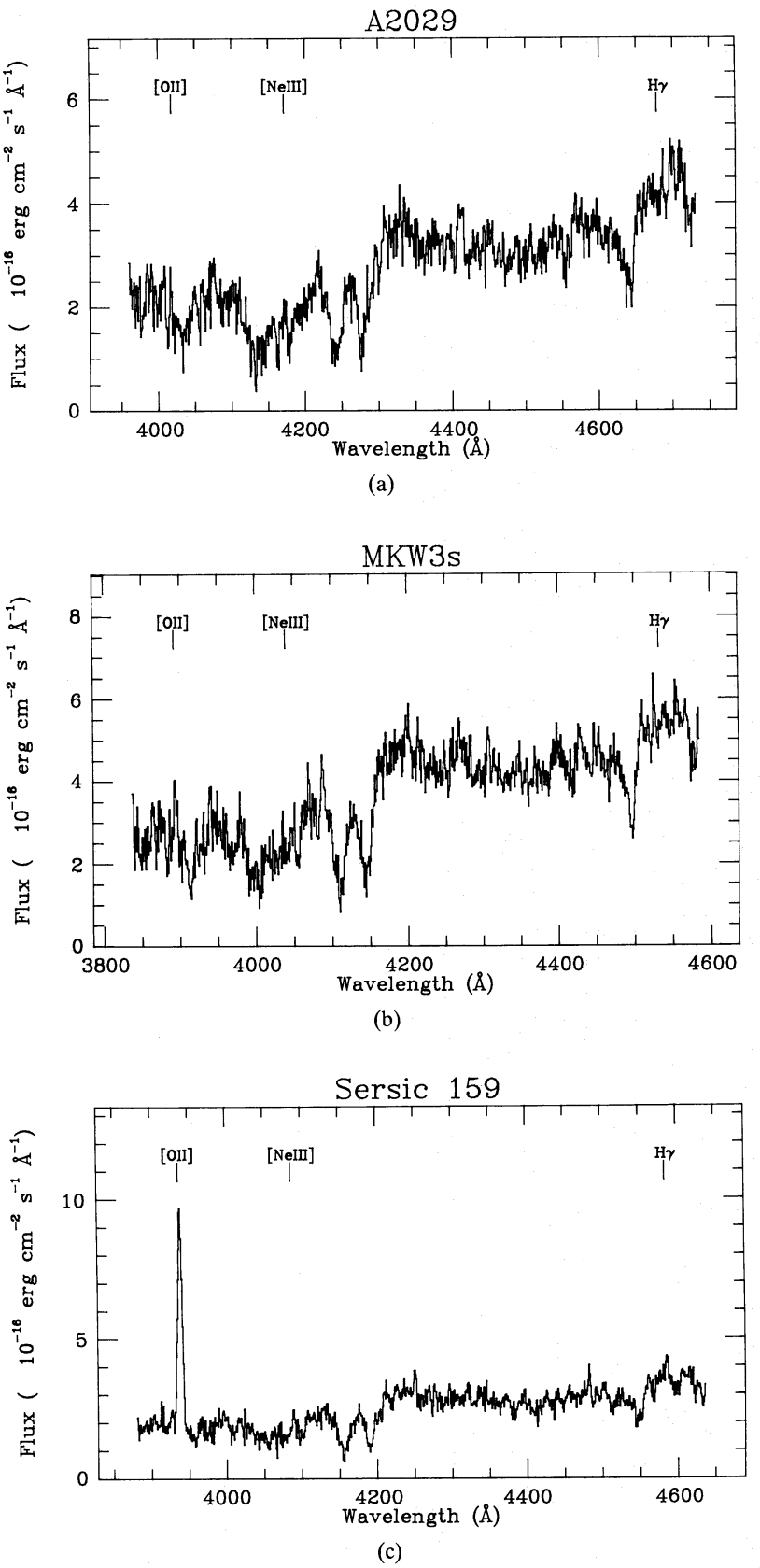

Figure 1. Part of the blue spectra of (a) A2029, (b) MKW3s and (c) Sersic 159 (slit position angle 0°) in the region of [O II] λ3727 and the 4000-Å break. Mass flow rates are 456 $M_\odot$ yr^{-1}, 126 $M_\odot$ yr^{-1} and 110 $M_\odot$ yr^{-1} respectively. The expected positions of some emission lines are marked.

2.3 MEASUREMENTS

2.3.1 Redshifts

Redshifts for the objects with blue spectra were measured by cross-correlation against the spectrum of NGC 4261 using the method of Tonry & Davis (1979). This object was the nearest elliptical that we observed and is at a redshift of $z=0.00754$ (in the observed frame). There is no obvious sign of emission lines. The spectra were prepared by selecting the wavelength region between [O II] and Hβ, in order to avoid the most intense emission lines in the spectrum. A simple pseudo-continuum, derived by running a recursive median filter (Martin & Lutz 1979) through the data, was subtracted before cross-correlation. The velocities, corrected to the frame of reference defined by the Local Group, are given in Table 1 together with the derived distances (we use $H_0=50\,\mathrm{km\,s^{-1}\,Mpc^{-1}}$).

2.3.2 Emission lines

2.3.2.1 Blue spectra. In some objects the emission lines are very prominent, in many they are weak and in others they are uncertain since a gap between absorption blends can mimic the appearance of a weak emission feature (see also Caldwell 1984). This underlying stellar absorption must be taken into account in order to obtain an accurate measure of the line fluxes. We have therefore adopted the technique of subtracting a redshifted template galaxy spectrum and measuring the residual spectrum. NGC 4261 was again used as the template. In order to work around the problem of the continuum shape being different in different objects, we used the following procedure to match the continuum shape of NGC 4261 to each galaxy in turn. A set of standard continuum windows was defined at zero redshift so that they did not include the wavelengths of common emission lines. These were redshifted by an amount corresponding to each galaxy in turn. Up to 13 cubic splines were fitted to the galaxy spectrum in these windows. This defined the continuum. The same procedure was then applied to the spectrum of NGC 4261 after it had been shifted to match the redshift of the galaxy. NGC 4261 was then multiplied by the ratio of the two spline continua before being subtracted from the galaxy spectrum. NGC 4261 does have an apparently high point at the redshifted wavelength of [O II], but by comparison with the objects NGC 6876, NGC 7626, A2670 and NGC 4760, which have a similar feature at a similar strength, and spectra at similar resolution of normal elliptical galaxies and globular clusters reported by Rose (1985), it seems likely that this feature is a gap between absorption blends rather than the [O II] emission line. It should be noted, however, that cooling flows involving up to $1\,M_\odot\,\mathrm{yr}^{-1}$ are common in elliptical galaxies (Nulsen, Stewart & Fabian 1984; Thomas *et al.* 1986) as are emission lines (Caldwell 1984; Phillips *et al.* 1986). Our emission-line fluxes are therefore, at worst, lower limits on the flux. To maximize the contrast between the emission lines and the continuum we binned up the data to match an FWHM of $300\,\mathrm{km\,s^{-1}}$. The measured emission-line fluxes and upper limits were derived by simply integrating under the line profile in an extracted spectrum covering the emission. Linewidths were measured by fitting a Gaussian plus a constant background to the corrected data. These quantities are given in Table 2. Table 3 lists the measured Hβ emission-line fluxes and linewidths from the very extended emission seen in some objects.

Our spatially resolved spectra of PKS 0745−191 have been presented by Fabian *et al.* (1985), and a detailed study and discussion of PKS 1404−267 is in preparation in collaboration with J. Danziger, R. Fosbury and others. We include those galaxies here for comparison with other galaxies.

2.3.2.2 Red spectra. The signal-to-noise ratio in these data is generally low. We have therefore binned the data to match an FWHM of $300\,\mathrm{km\,s^{-1}}$ before measuring the line fluxes. As no galactic

Table 2. Hβ line fluxes and velocity widths for central emission.

Object	Cross Sections	Hβ Flux	Hβ Width	Position Angle
PKS0745-191	24-30	518	351±137	55
	25-31	767	429±320	145
A1060	25-30	<5.9		
NGC4261	25-31	<0.43		
NGC4696	25-30	46	1034±299	
NGC4760	25-31	<36		
IC4296	26-31	<39		
PKS1404-267	26-30	63	948±200	110
	26-30	70	1024±383	200
A1991	25-31	5.5	too weak	
A2029	25-30	<6.2		
MKW3s	25-30	11		
A1795	23-28	53	508± 46	
IC4765	25-30	<38		
NGC6876	12-17	<12		
2103-45	25-30	<24		
2215-359	25-31	not covered		
NGC7385	25-30	<16		
Sersic 159	25-30	18	445± 75	65
	25-30	10	196± 70	0
NGC7626	25-30	<33		
A2626	25-30	6.7	92± 24	
A2670	25-30	<85		
A85	25-30	<23		

Fluxes are in units of 10^{-16} erg cm^{-2} s^{-1}. Velocities are in km s^{-1}. Each cross-section corresponds to 2.2 arcsec along the slit.

Table 3. Hβ line fluxes and velocity widths for very extended emission.

Object	Cross Sections	Hβ Flux	Hβ Width	Position Angle
PKS1404-267	21-25	13	187±118	110
A1991	23-24	1.0	~140	
A1795	15-22	12	97±100	
Sersic 159	20-24	3.5	238± 55	0

Fluxes are in units of 10^{-16} erg cm^{-2} s^{-1}. Velocities are in km s^{-1}. Each cross-section corresponds to 2.2 arcsec along the slit.

Table 4. Emission-line ratios.

Object	Cross Section	OII / Hβ	NeIII / Hβ	NeIII / Hγ	Hγ / Hβ	OIII / Hβ	OIII / Hβ	OI / Hα	NII / Hα	SII / Hα	Position Angle
		3727	3869	3968	4340	4959	5007	6300	6584	6720	
PKS0745-191	24-30	11	0.5	0.8	0.5	0.3	1.2				55
	25-31							1.3	0.5		55
	25-31	8.7	1.4	0.9	0.4	0.3	0.8				145
NGC4696	25-30	2.3	0.6	0.5	0.2	0.2	0.3				
	23-29							<1.0	3.2	1.5	167
PKS1404-267	26-30	2.4	0.3	0.5	0.1	0.1	0.9				110
	21-25	3.0	0.2	0.5	<0.2	<0.2	0.2				110
	26-30	1.0	0.3	0.3	0.1	0.3	0.9				200
	25-30							<1.0	4.0	1.5	110
	21-24							<1.0	2.8	<1.0	110
A1991	25-31	1.1	<1.0	<1.0	<1.0						
	23-24	7.1	<1.0	<1.0	<0.5						
MKW3s	25-30	1.2	<1.0	<1.0	<1.0	<1.0	<1.0				
A1795	23-28	3.3	2.0?	0.2	0.2	0.3	0.4				160
	15-22	2.1	<1.0	1.4?	0.5	<0.3	<0.3				160
	25-30							0.6	1.6	1.1	170
IC4765	25-30	0.7	<1.0	<1.0	<1.0	<1.0	<1.0				
NGC7385	25-30	>0.7									
SC2028-566	24-30						<0.2	0.9	0.4		
Sersic 159	25-30	3.1	0.7	0.3	0.2	0.5	0.5				65
	25-30	5.9	0.4	0.5	0.4	0.1	0.4				0
	24-30							0.3	2.1	0.7	240
A2626	25-30	2.2	<1.0	<1.0	<1.0	<1.0	<1.0				
A85	24-31							<1.0	2	<1.0	

Line ratios are given for individual lines, except in the case of O II, N II and S II where the ratio is that for both components of the doublet. Values marked ? are very uncertain. We find similar line ratios for the two objects (A1795 and A85) which are in common with the work of Hu *et al.* (1985).

absorption features are generally discernible in the spectra, the fluxes were measured by simply integrating under the sky-subtracted spectrum in the region of the lines. Emission-line ratios are given in Table 4. These spectra were not flux calibrated, but line ratios are not grossly affected since the wavelength range of interest covered within an individual spectrogram is small (<500 Å).

2.3.3 4000-Å breaks

The 4000-Å break D is the ratio of the continuum intensity in a band from 4050 to 4250 Å to that in a band from 3750 to 3950 Å. We use the definition given by Bruzual (1983):

$$D=\left(\int_{4050}^{4250} F_\nu\, d\lambda\right)\Big/\left(\int_{3750}^{3950} F_\nu\, d\lambda\right).$$

Table 5. 4000-Å breaks.

Object	Central Break	Total Break	Position Angle	Object	Central Break	Total Break	Position Angle
PKS0745-191	1.03	1.41	55	A1795	1.37	1.19	
	0.93	1.32	145	IC4765	2.42	2.39	
A1060	2.07	2.02		NGC6876	2.54	2.45	
NGC4261	2.40	2.34		2103-45	2.25	2.27	
NGC4696	2.26	2.27		2215-359	2.38	2.48	
NGC4760	2.20	2.17		NGC7385	2.19	2.02	
IC4296	2.40	2.35		Sersic 159	1.82	1.89	65
PKS1404-267	2.13	2.09	110		1.83	1.93	0
	2.34	2.13	200	NGC7626	2.52	2.39	
A1991	1.95	2.03		A2626	1.92	2.01	
A2029	2.02	2.08		A2670	2.09	2.10	
MKW3s	2.02	1.93		A85	1.91	1.84	

The strength of this feature decreases systematically from late-type to early-type stars and so is a diagnostic of the underlying stellar population. Measurements of D from our blue spectra are presented in Table 5. Two figures are given, one for the central region of the galaxy and one for the whole of the detected galaxy. There are indications of significant small variations of D across some of our galaxies. Confirmation of this requires further observations in which the effects of S-distortion in the IPCS can be calibrated out.

3 Analysis

In this section we shall relate the optical properties of the cooling flows to the mass flow rate $\dot{M}$ deduced from the imaging X-ray data. These observations show that $\dot{M}$ systematically increases with radius r within the region where $t_{\rm cool}<H_0^{-1}$. Roughly, $\dot{M}\propto r$ (Fabian, Arnaud & Thomas 1986b). Earlier work in this field (e.g. Stewart *et al.* 1984) listed the mean mass flow rate while, more recently, total mass flow rates integrated over the entire cooling region have been given (e.g. Arnaud 1985). We denote this total rate as $\dot{M}_{\rm x}$. The cooling region in a typical cluster is about 100–300 kpc in diameter whereas optical line emission is detected within a much smaller region of diameter 10–20 kpc. The integrated mass flow rate deduced from the X-ray data within this region is denoted $\dot{M}_{\rm v}$, and is generally much less than $\dot{M}_{\rm x}$. We estimate $\dot{M}_{\rm v}$ by first calculating the radius $r_{\rm v}$ of a circular aperture which would have the same area as that part of our spectrograph slit in each extracted spectrum. Then

$$\dot{M}_{\rm v}\approx\dot{M}_{\rm x}\frac{r_{\rm v}}{r_{\rm cool}},$$

where $r_{\rm cool}$ is the radius at which the cooling time equals the Hubble time. Because of the simple scaling, values of $\dot{M}_{\rm v}$ are uncertain by a factor of about 2. We assume that once the gas cools from the X-ray emitting temperatures it collapses into stars before falling further into the galaxy; i.e. below 10^6 K, $t_{\rm cool}\ll t_{\rm dyn}$, where $t_{\rm dyn}$ is the local free-fall time.

3.1 COMPARISON OF Hβ LUMINOSITY WITH $\dot{M}$

As gas cools from above 10^6 K to below 10^3 K it recombines and emits Balmer photons. The luminosity in a recombination line such as Hβ is therefore related to $\dot{M}$ by (Cox 1972)

$$L(\mathrm{H}\beta)=9.3\times10^{36}\,H_{\mathrm{rec}}\,\dot{M}\,\mathrm{erg\,s^{-1}}, \quad (1)$$

where $\dot{M}$ is in solar masses per year and H_{rec} is the number of times that each hydrogen ion recombines. The value of H_{rec} depends upon the local photo-ionizing and heat flux. In the absence of other heat sources, the photo-ionizing flux from gas cooling above 10^6 K is very similar to that formed behind an interstellar shock (Binette, Dopita & Tuohy 1985). Indeed, shocks do form in rapidly cooled blobs if they are large since they fall out of pressure balance (Cowie, Fabian & Nulsen 1980). In these cases H_{rec} is between 1 and 2 for models which match the observed optical line ratios (Raymond 1979).

The predicted Hβ luminosity is then

$$L(\mathrm{H}\beta)\approx10^{39}\,\dot{M}_{100}\,\mathrm{erg\,s^{-1}}, \quad (2)$$

where $\dot{M}=100\,\dot{M}_{100}\,M_\odot\,\mathrm{yr}^{-1}$. This is generally undetectable at the distances of most cooling flows, especially if it is spread fairly uniformly over a region 100–300 kpc in diameter. The apparent lack of optical line emission in A2029 therefore does not rule out a cooling flow. Observed values of $L(\mathrm{H}\beta)$ are plotted against $\dot{M}_{\mathrm{x}}$ and $\dot{M}_{\mathrm{v}}$ in Fig. 2(a) and (b) respectively. The values of H_{rec} corresponding to $\dot{M}_{\mathrm{x}}$ and $\dot{M}_{\mathrm{v}}$ are also given in Table 6. The straight line represents equation (2). In both figures the points all lie well above this relation. It is therefore clear that the lack of detectable emission from A2029 relative to objects with similar mass flow rates does not contradict the presence of a cooling flow with the rate inferred from the X-ray data.

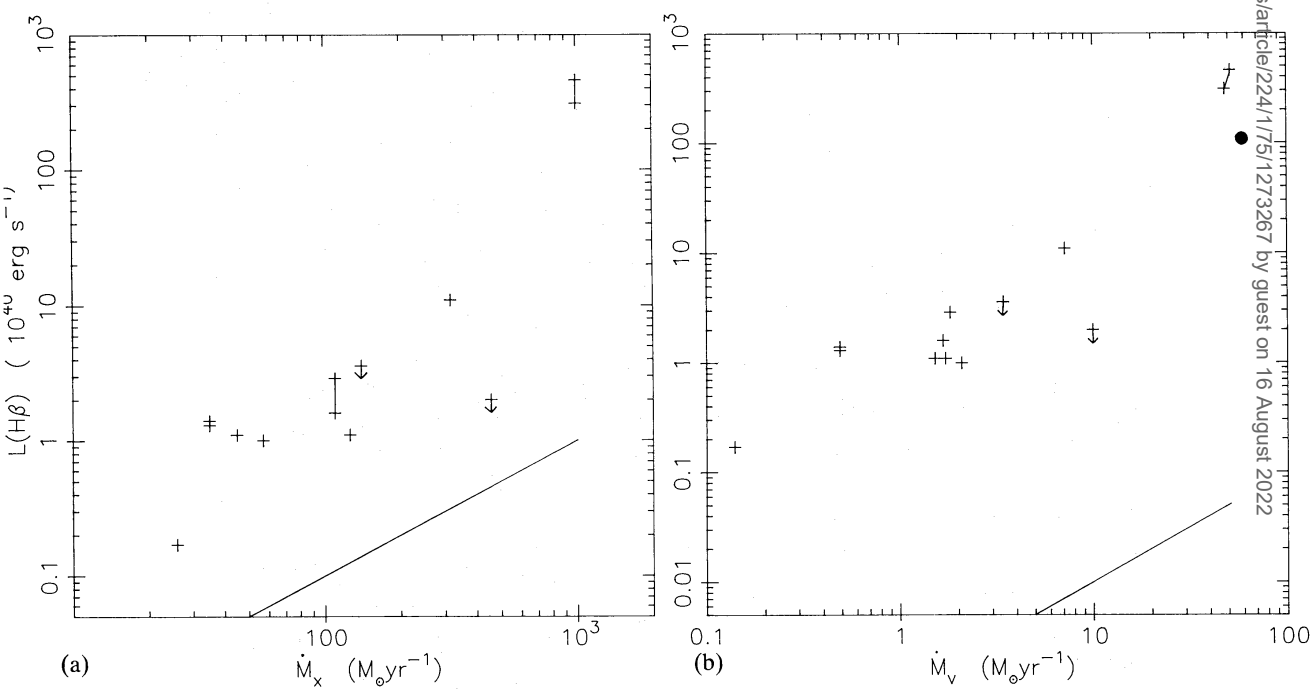

Figure 2. (a) Hβ luminosity as a function of the total integrated mass flow rate $\dot{M}_{\mathrm{x}}$ for all the cooling flows observed [the straight line represents the expected Hβ luminosity at a given mass flow rate according to equation (2); points corresponding to the same object are joined]; (b) Hβ luminosity as a function of mass flow rate $\dot{M}_{\mathrm{v}}$ within the spectrograph slit for all the cooling flows observed [the straight line represents the expected Hβ luminosity at a given mass flow rate, given by equation (2); points corresponding to the same object are joined; we have estimated the position of NGC 1275 from the data of Hu *et al.* (1983) and plotted it as a full circle].

Table 6. Hβ luminosities, mass flow rates and H_{rec} for cooling flows.

Object	Cross Section	L(Hβ)	$\dot{M}_x$	$H_{rec,x}$	$\dot{M}_v$	$H_{rec,v}$	Position Angle
PKS0745-191	24-30	3.1E42	1000[1]	333	48.1	6930	55
	25-31	4.6E42	1000[1]	495	51.4	9620	145
NGC4696	25-30	1.7E39	26[2]	7.0	0.14	1310	
PKS1404-267	26-30	1.3E40	35[2]	39.9	0.49	2850	110
	26-30	1.4E40	35[2]	43.0	0.49	3070	200
A1991	25-31	1.0E40	57[3]	18.9	2.08	517	
A2029	25-30	<2.0E40	456[4]	<4.72	9.96	<216	
MKW3s	25-30	1.1E40	126[2]	9.4	1.72	688	
A1795	23-28	1.1E41	316[3]	37.4	7.15	1654	
Sersic 159	25-30	2.9E40	110[4]	38.3	1.82	1710	65
	25-30	1.6E40	110[4]	15.6	1.82	945	0
A2626	25-30	1.1E40	45[3]	26.3	1.52	778	
A85	25-30	<3.6E39	140[3]	<27.6	3.43	<1129	

Values of $\dot{M}_x$ and r_{cool} are taken from the following.
[1]Fabian *et al.* (1985).
[2]Our own unpublished data.
[3]Arnaud (1985).
[4]This work.

The existence of detectable line emission is not simply explained and merits further study. We require $2 \lesssim H_{rec} \lesssim 500$ (Table 6) using $\dot{M}_x$, and between one and two orders of magnitude larger using $\dot{M}_v$.

Hu *et al.* (1983) explain the large optical line flux from NGC 1275 in the Perseus cluster as resulting from a gaseous collision with the intervening 8000 km s^{-1} system, which is presumed to be a galaxy falling through the cluster core. Although this may account for the energy emitted, the mechanism of energy transfer is unspecified and there is already enough energy in the hot gas since the optical flux represents less than 1 per cent of the X-ray luminosity. Using their data, we have plotted the position of NGC 1275 on Fig. 2(b) as a full circle. It appears to follow the trend of the other cooling flow galaxies, and so is not exceptional. We therefore doubt that their explanation is correct.

The basic problem arising when it is assumed that the only source of heat is from photo-ionization by the cooling gas is that it can only balance radiative cooling in optically emitting gas over a narrow temperature range around 8000 K where hydrogen recombines. The photons just shortward of 912 Å are primarily responsible for the photo-ionization, and equilibrium is achieved only over a very thin region of about unit photoelectric absorption depth at those wavelengths. We have checked this (see also Binette *et al.* 1985) using Ferland's code (Ferland & Truran 1981) with a photo-ionization spectrum consisting of a weighted sum of Raymond & Smith (1977) spectra for gas cooling between 10^7 and 10^5 K. The weights were set proportional to the value of the cooling function at each temperature to take account of the change in the cooling time as the gas cools. We obtain an ionized region which is less than 2000 AU thick and which radiates only a few per cent of the luminosity that we require to match our data.

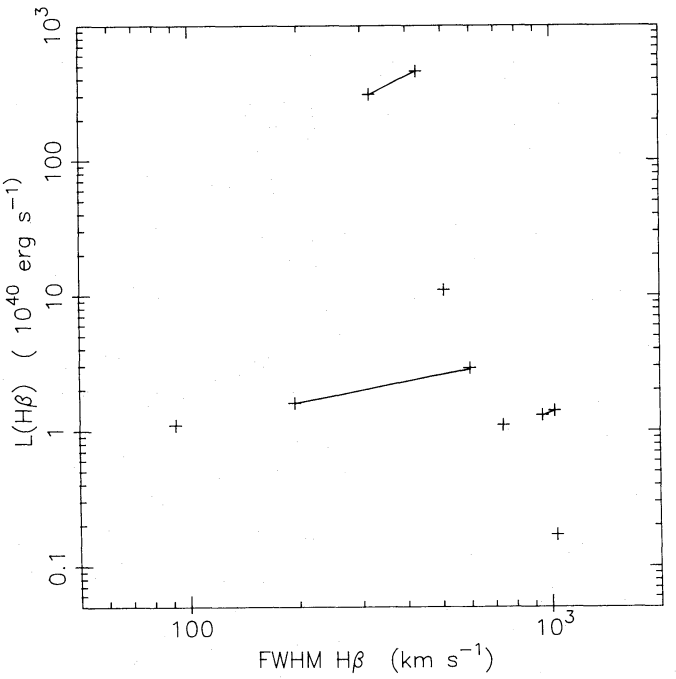

Figure 3. Comparison of Hβ luminosity with the FWHM of the Hβ line. Points corresponding to the same object are joined.

For this same reason we can also rule out Miller's (1986) explanation of the optical line radiation in which the gas is maintained at about 10^4 K by photo-ionization from the surrounding gas.

To explain the luminosity observed we require that the gas remains in the ionized region for 100–1000 times longer than indicated by the simple photo-ionization model. Some extra form of ionization is therefore required. We stress that the observed line ratios are in good agreement with those predicted by photo-ionization from the cooling gas (Raymond 1979; Binette *et al.* 1985).

Some possible sources of extra ionization are (1) continued shocks, (2) conduction, (3) cosmic rays and (4) an active nucleus. None of these provides a satisfactory explanation. The collapse of a complex large blob and the dissipation of turbulence in the cooling gas could lead to continued shocks and account for the relatively large optical linewidths. The subsonic inflow leads to velocity widths of tens of kilometres per second whereas velocities of several hundred kilometres per second are common. The kinetic energy in the line-emitting gas represents a significant fraction of the optical luminosity, but it is not clear that it can give $H_{\rm rec}$=1000. Fig. 3 shows the luminosity in Hβ plotted against the FWHM of the Hβ line, for our data. There is no obvious correlation.

Conduction, cosmic rays and an active nucleus have each been considered and rejected by Cowie *et al.* (1983), Fabian, Nulsen & Canizares (1982) and Kent & Sargent (1979) respectively. Our preferred explanation is discussed in Section 3.2.

3.2 STAR FORMATION

Most of $\dot{M}_{\rm x}$ cannot continually form stars with the initial mass function (IMF) of a disc galaxy without making the underlying galaxy too bright and too blue (Fabian *et al.* 1982; Sarazin & O'Connell 1983; Romanishin 1985). However, some young stars are required to explain the A- and F-type optical spectra of NGC 1275 (Rubin *et al.* 1977) and the central galaxy in A1795 (Sarazin 1986) respectively. The ultraviolet spectra of M87 (Bertola, Capaccioli & Oke 1982) and

NGC 6166 (Bertola *et al.* 1986), which are both at the centres of cooling flows, also indicate the presence of a population of hot stars, probably young OB stars. The general assumption that elliptical galaxies contain only old stars has been in question for some time (e.g. van den Bergh 1975). Recent studies show that a low level of continuous star formation may occur in most elliptical galaxies (Pickles 1985). We now consider the rate of formation of hot stars in our galaxies.

The 4000-Å breaks D for our galaxies are listed in Table 5. This quantity is a measure of the number of young stars in the underlying population. We find a clear trend (Fig. 4) when D is plotted against $\dot{M}_v$ such that a higher mass flow indicates a smaller break, i.e. more hot (and therefore young) stars. A Spearman rank correlation test (Siegel 1956) confirms this at the 1 per cent level (single-sided confidence region).

Star formation with a disc galaxy IMF is relatively efficient at producing ionizing photons from the Lyman continuum of the massive stars (above $40\,M_\odot$). The Hβ luminosity $L(\mathrm{H}\beta)$ thereby produced is about $4\times10^{40}\,\mathrm{erg\,s^{-1}}\,M_\odot^{-1}\,\mathrm{yr}$ (Kennicutt 1983) and corresponds via equation (1) to $H_{\rm rec}\approx4\times10^3$. Consequently we require that only 0.1–10 per cent of $\dot{M}$ forms stars with a disc galaxy IMF in order to produce the observed Hβ flux, $F(\mathrm{H}\beta)$. A direct consequence of this is that the Hβ flux should correlate with the presence of massive stars as measured by the 4000 Å break D. To estimate this we have used Kennicutt's approximation to the IMF of a disc galaxy:

$$\frac{dN}{dm\,dt}=0.5\begin{cases}m^{-1.4} & 0<m<1\,M_\odot\\ m^{-2.5} & 1<m<60\,M_\odot\end{cases} \tag{3}$$

where N is the number of stars produced per unit mass $m/M_\odot$ per year. The total luminosity produced by $1\,M_\odot\,\mathrm{yr}^{-1}$ of star formation above and below the breaks 4050–4250 Å (subscript A) and 3750–3950 Å (subscript B) is then

$$\frac{L_{\mathrm{A,B}}}{\dot{M}}=\int_1^{60}\frac{dN}{dm\,dt}\,\tau(m)l_{\mathrm{A,B}}(m)\,dm, \tag{4}$$

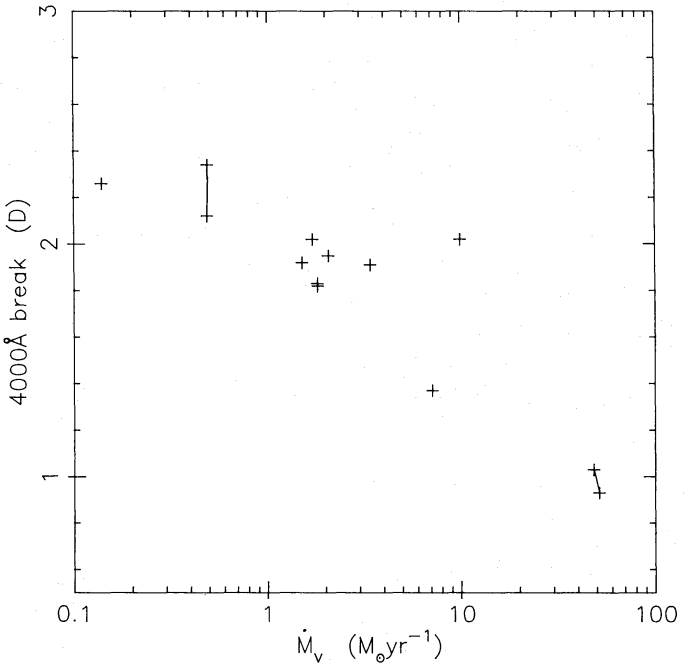

Figure 4. Magnitude of the 4000-Å break D plotted against the mass flow rate $\dot{M}_v$ within the spectrograph slit for all the cooling flows observed. Points corresponding to the same object are joined.

where $\tau(m)$ is the main-sequence lifetime and $l_{A,B}(m)$ is the band luminosity of a star of mass m. We approximate $\tau(m)$ from the tabulations by Bruzual (1981), and $l_{A,B}(m)$ by summing over the appropriate range in the model atmospheres of Kurucz (1979):

$$L_A = 6.76\times10^{41}\,\mathrm{erg\,s^{-1}}\,M_\odot^{-1}\,\mathrm{yr}, \tag{5a}$$

$$L_B = 6.06\times10^{41}\,\mathrm{erg\,s^{-1}}\,M_\odot^{-1}\,\mathrm{yr}. \tag{5b}$$

The break D due to stars above $1\,M_\odot$ is thus 1.12. Stars of spectral type B and A dominate L_B, as expected.

We have ignored the evolution of the stars into giants, which have larger values of D (about 2.5). This is only important for the stars of mass about $1\,M_\odot$ as the horizontal branch lifetime of more massive stars is very short. The former are assumed to be represented by our template galaxies, which show no sign of star formation. Let D for a template galaxy be D_T and its 4050–4250 Å flux be F_{TA}. Similarly, represent these parameters for another observed galaxy by D_0 and F_A and the contribution from young stars by D_* and F_{*A}. Then, above and below the break,

$$F_A = F_{TA} + F_{*A} \tag{6a}$$

$$F_B = F_{TB} + F_{*B}. \tag{6b}$$

Rearranging and eliminating F_T, we obtain

$$F_{*A} = F_A(D_0^{-1} - D_T^{-1})(D_*^{-1} - D_T^{-1})^{-1}. \tag{7}$$

Finally, using equation (5a), $D_T = 2.41$, D_* and the distance d, we can directly relate F_{*A} to the star formation rate $\dot{M}_D$, with a disc galaxy IMF within our spectrograph aperture:

$$\dot{M}_D = 3\times10^{-42}F_A(D_0^{-1} - 0.41)4\pi d^2(1+z)^2. \tag{8}$$

The redshift is assumed to be small. This should be compared with the star formation rate inferred from the Hβ flux using Kennicutt's (1983) formula:

$$\dot{M}_{H\beta} = 2.5\times10^{-41}F(H\beta)4\pi d^2(1+z)^2. \tag{9}$$

In order to remove any spurious correlation due to distance, we plot $0.03F_A(D_0^{-1} - 0.41)$ against $0.25F(H\beta)$ in Fig. 5. The straight line has a slope of unity. The above relations include normalizations such that the galaxies would lie on this line if all the Hβ luminosity were generated by the Lyman continuum from the OB stars expected from the weakening of the 4000 Å break and a disc galaxy IMF. Good agreement is found for most of the galaxies. The weaker 4000 Å break observed within those galaxies with Hβ emission agrees quantitatively with the star formation hypothesis.

$\dot{M}_{H\beta}$ is plotted against $\dot{M}_v$ in Fig. 6. Again, the straight line has a slope of unity. This shows that the X-ray data from a region of comparable size to our aperture yield a mass deposition rate comparable with, or in excess of, the star formation rate deduced from the Hβ luminosity. Note that $\dot{M}_D$ and $\dot{M}_{H\beta}$ correspond to the same aperture and that the relatively small wavelength range used for the 4000 Å break means that any problems with flux correction or differential flux loss are minimized.

Our data therefore provide strong evidence for the formation of hot stars in cooling flows. Between 0.05 and $100\,M_\odot\,\mathrm{yr}^{-1}$ of star formation with a disc galaxy IMF is proceeding, while the remainder of $\dot{M}_x$ presumably collapses and forms objects of much lower mass. Such behaviour can be explained if high pressure is a strong factor in creating very-low-mass objects (Jura 1977). The X-ray emitting gas is likely to contain a range of densities on all scale sizes. The densest regions cool most rapidly through thermal instability. If their size is small enough for the sound crossing

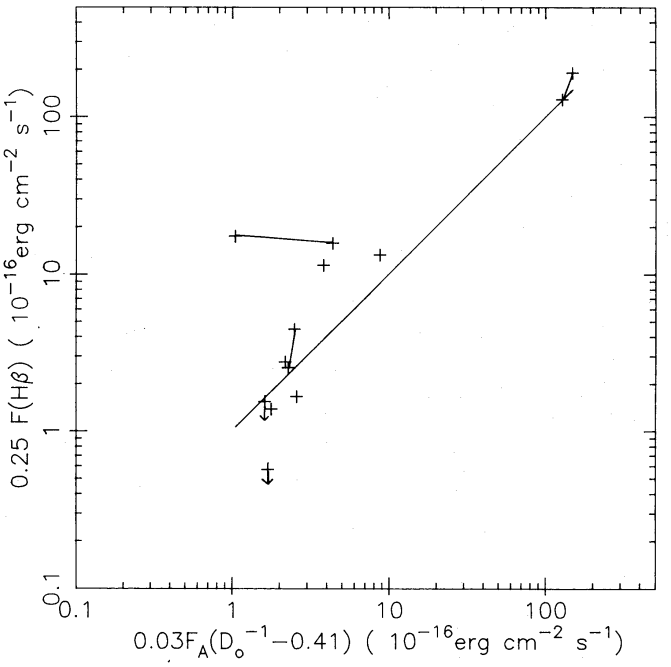

Figure 5. Comparison of the weakening of the 4000-Å break with the Hβ flux for cooling flows. Both of these measure the star formation rate and should be proportional to each other. The line has a slope of unity. Points corresponding to the same object are joined. Errors on the abscissae are a strong function of the x-value. For a typical error of 5 per cent in D, the errors in $\dot{M}_D$ are 137 per cent, 28 per cent, 13 per cent and 9 per cent for D values of 2.35, 2.0, 1.5 and 1.0 respectively.

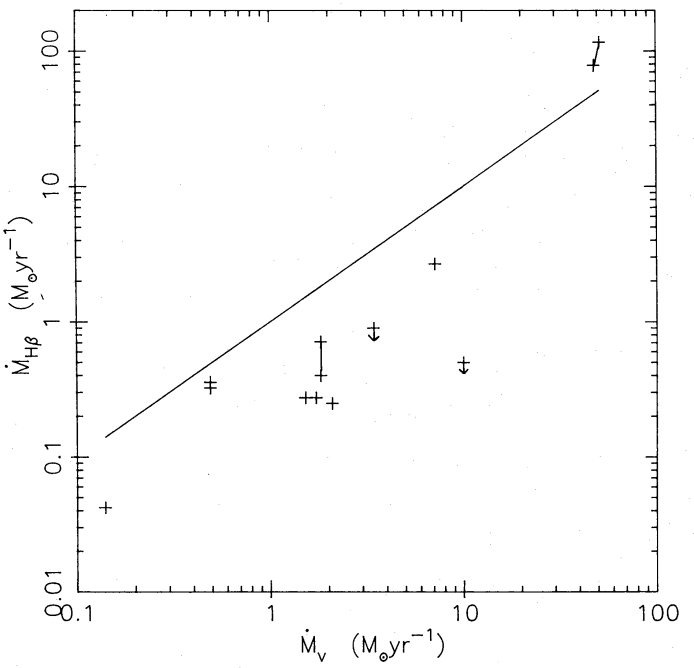

Figure 6. Comparison of $\dot{M}_{H\beta}$ with $\dot{M}_v$. The straight line has a slope of unity and shows that the star formation rate deduced from X-ray data is comparable with, or in excess of, that deduced from the luminosity in Hβ. Points corresponding to the same object are joined.

time to be less than the cooling time, they remain in pressure equilibrium with the surrounding high-pressure gas and form low-mass objects. However, blobs larger than about 1 kpc cool isochorically from 10^6 K and reach 10^4 K with interior pressures that are only 1 per cent of that in the rest of the gas (Cowie *et al.* 1980). Small blobs embedded within such large blobs can then collapse at relatively low pressure and so form high-mass stars (Fabian *et al.* 1986a).

As a final check on star formation we have estimated the Lyman continuum of the massive stars from the model atmospheres of Kurucz (1979) and added it to the X-ray and ultraviolet flux from the cooling gas used in our photo-ionization calculation (see Section 3.1). The line ratios are similar to those obtained from a high-velocity shock but with much higher fluxes, in closer agreement with those observed in our galaxies. The relative intensities of the stellar and cooling fluxes depend upon the geometry of the blobs and further work may allow this to be constrained (e.g. spheres or sheets).

4 Discussion

4.1 REDDENING

We have ignored any possible reddening due to dust within the cooling flow. Dust is expected to be absent from the immediately cooled gas (Draine & Salpeter 1979) but may be formed in the outer atmospheres of stars. Infrared observations of NGC 1275 reported by Gear *et al.* (1985) indicate that there is some dust, although they find that star formation with a disc galaxy IMF accounts for only a few per cent of the X-ray inferred mass flow rate. This is consistent with the ultraviolet continuum limit on hot stars obtained by Fabian, Nulsen & Arnaud (1984) and the estimates for disc galaxy IMF star formation discussed in Section 3.

4.2 SUPERNOVAE

Star formation with a disc galaxy IMF will produce supernovae which are a further source of heat. Scaling from our Galaxy, where the supernova rate is about one per 30 yr and the star formation rate is about four per year (Smith, Biermann & Mezger 1978), we estimate that supernovae of energy 10^{51} erg generate the same power as is radiated by $1\,M_\odot\,\mathrm{yr}^{-1}$ cooling from 5×10^7 K. Consequently, as the disc galaxy IMF star formation rate in most of the cooling flows is less than or similar to that in our Galaxy, the heat injected by supernovae seriously affects less than 1 per cent of the total flow. Supernovae are expected at the rate of about one per 10–100 yr. Only in PKS 0745−191 does the predicted rate approach one per year. Again, supernovae will have little effect on most of the thermally unstable cooling gas.

4.3 GLOBULAR CLUSTERS

We note that the ionizing radiation from hot stars will delay the cooling of gas at 10^4 K in the large blobs by a factor of about 100. Such blobs will have a mass of about $10^6\,M_\odot$ and can become gravitationally unstable at that temperature. This provides a promising explanation for the formation of the large number of globular clusters observed in nearby cooling flows (Fabian, Nulsen & Canizares 1984; Fall & Rees 1985).

4.4 A COMPARISON OF Sersic 159 AND A2029

Sersic 159 and A2029 are very similar clusters at X-ray wavelengths. Deprojecting the X-ray surface brightness using the technique of Fabian *et al.* (1981, 1985), we estimate a total mass

deposition rate of $110\,M_\odot\,yr^{-1}$ for Sersic 159 and $456\,M_\odot\,yr^{-1}$ for A2029. The optical spectra of their central galaxies are quite different (see Fig. 1), however, Sersic 159 shows line emission [note that Charles & Phillips (1982) failed to detect that strong flux] with $L(O\,II)=9.3\times10^{40}\,erg\,s^{-1}$, whereas a limit of $L(O\,II)<4.9\times10^{40}\,erg\,s^{-1}$ can be placed on A2029. Their 4000-Å breaks are nevertheless similar (1.9 and 2.0 respectively).

The above difference between Sersic 159 and A2029 raises several points. As discussed earlier, our luminosities and limits apply to only a very small region of the total flow, a few kiloparsecs in radius (except in the case of PKS 0745−191). If the optical line flux varies so that $L(H\beta)\propto\dot{M}_x$ at all radii within r_{cool}, the total line luminosities could be an order of magnitude greater than those listed in Table 6. Whether we detect optical line emission then depends on how peaked that emission is. Furthermore, if the identification of the site of hot stars with large blobs (Section 3.2) is correct, the presence of detectable line emission depends, through these stars, on the presence of large blobs. Motions and stripping of other galaxies may help to generate large blobs, whereas motion of the central galaxy (e.g. slow oscillation in the bottom of the cluster potential well) should break them up. Consequently, the formation of hot stars may be very patchy in cooling-flow galaxies. The lifetime of large blobs is probably not much more than 10^7 yr (the lifetime of the ionizing stars), whereas the B and A stars responsible for the 4000-Å break live from 10^8 to 10^9 yr so that they may be observed in regions devoid of line emission. Examples of this may be the blue 'loop' in NGC 1275 noted by Sandage (1971) and the continuum 'filaments' in A496 (Fabian *et al.* 1982; see discussion in Cowie *et al.* 1983). We attribute the scatter in Figs 4–6 to variations in the proportion of the mass deposition rate that occurs near the centre of the flow through large blobs. A2029 is then just an extreme example of this phenomenon.

5 Conclusions

Strong extended optical line emission appears to be common around the central galaxies in cooling flows. Our studies of the blue part of the spectrum, in particular the 4000-Å break and Hβ flux, show that some star formation takes place with an IMF similar to that of disc galaxies. This generally corresponds to less than 1 per cent of the X-ray inferred mass deposition rate. In one extreme case, PKS 0745−191, it approaches 10 per cent, or $100\,M_\odot\,yr^{-1}$. The bulk of the cooling gas, in all cases, must collapse into low-mass objects so that the IMF for the whole galaxy is strongly skewed towards lower masses.

We have suggested that the detectable line emission is associated with the largest blobs in the flow. Most of the gas is presumably not in large blobs and produces at most only one Hβ photon per proton. This is undetectable at the present time.

Acknowledgments

We thank Keith Arnaud for supplying the X-ray data on Sersic 159 and A2029 and John Danziger for informing us of PKS 1404−267. RMJ and ACF acknowledge the support of a Science and Engineering Research Council postdoctoral fellowship and the Royal Society respectively.

References

Arnaud, K. A., 1985. *PhD thesis*, University of Cambridge, Cambridge.
van den Bergh, S., 1975. *Ann. Rev. Astr. Astrophys.*, **13,** 217.
Bertola, F., Capaccioli, M. & Oke, J. B., 1982. *Astrophys. J.*, **254,** 494.
Bertola, F., Gregg, M. D., Gunn, J. E. & Oemler, A., 1986. *Astrophys. J.*, **303,** 624.
Binette, L., Dopita, M. A. & Tuohy, I. R., 1985. *Astrophys. J.*, **297,** 476.
Bohlin, R. C., Savage, B. D. & Drake, J. F., 1978. *Astrophys. J.*, **224,** 132.

Bruzual, G. A., 1981. *PhD thesis*, University of California, Berkeley, CA.
Bruzual, G. A., 1983. *Astrophys. J.*, **273,** 105.
Caldwell, N., 1984. *Publs astr. Soc. Pacif.*, **96,** 287.
Charles, P. A. & Phillips, M. M. 1982. *Mon. Not. R. astr. Soc.*, **200,** 263.
Cowie, L. L., Fabian, A. C. & Nulsen, P. E. J., 1980. *Mon. Not. R. astr. Soc.*, **191,** 399.
Cowie, L. L., Hu, E. M., Jenkins, E. B. & York, D. G., 1983. *Astrophys. J.*, **272,** 29.
Cox, D. P., 1972. *Astrophys. J.*, **178,** 153.
Draine, B. T. & Salpeter, E., 1979. *Astrophys. J.*, **231,** 77.
Fabian, A. C., Arnaud, K. A., Nulsen, P. E. J. & Mushotzky, R. F., 1986a. *Astrophys. J.*, **305,** 9.
Fabian, A. C., Arnaud, K. A., Nulsen, P. E. J., Watson, M. G., McHardy, I., Smith, A., Cooke, B., Elvis, M. & Mushotzky, R. F., 1985. *Mon. Not. R. astr. Soc.*, **216,** 923.
Fabian, A. C., Arnaud, K. A. & Thomas, P. A., 1986b. *Proc. IAU Symp. 117,* in press.
Fabian, A. C., Hu, E. M., Cowie, L. L. & Grindlay, J., 1981. *Astrophys. J.*, **248,** 47.
Fabian, A. C., Nulsen, P. E. J. & Arnaud, K. A., 1984. *Mon. Not. R. astr. Soc.*, **208,** 179.
Fabian, A. C., Nulsen, P. E. J. & Canizares, C. R., 1982. *Mon. Not. R. astr. Soc.*, **201,** 933.
Fabian, A. C., Nulsen, P. E. J. & Canizares, C. R., 1984. *Nature,* **310,** 733.
Fall, S. M. & Rees, M. J., 1985. *Astrophys. J.*, **298,** 18.
Ferland, G. R. & Truran, J. W., 1981. *Astrophys. J.*, **244,** 1022.
Filippenko, A. V., 1982. *Publs astr. Soc. Pacif.*, **74,** 715.
Gear, W. K., Gee, G., Robson, E. I. & Nott, I. G., 1985. *Mon. Not. R. astr. Soc.*, **217,** 281.
Hu, E. M., Cowie, L. L., Kaaret, P., Jenkins, E. B., York, D. G. & Roesler, F. L., 1983. *Astrophys. J.*, **275,** L27.
Hu, E. M., Cowie, L. L. & Wang, Z., 1985. *Astrophys. J. Suppl. Ser.*, **59,** 447.
Jones, C. & Forman, W., 1984. *Astrophys. J.*, **276,** 38.
Jura, M., 1977. *Astrophys. J.*, **212,** 634.
Kennicutt, R. C. Jr, 1983. *Astrophys. J.*, **272,** 54.
Kent, S. M. & Sargent, W. L. W., 1979. *Astrophys. J.*, **230,** 667.
Kurucz, R. L., 1979. *Astrophys. J. Suppl. Ser.*, **40,** 1.
Martin, R. & Lutz, L. K., 1979. In: *International Workshop on Image Processing in Astronomy, Proc. 5th Colloq. on Astrophysics, Osservatorio Astronomico di Trieste,* p. 211, eds Sedmak, G., Capaccioli, M. & Allen, R. J.
Miller, L., 1986. *Mon. Not. R. astr. Soc.*, **220,** 713.
Nulsen, P. E. J., Stewart, G. C. & Fabian, A. C., 1984. *Mon. Not. R. astr. Soc.*, **208,** 185.
Oke, J. B., 1974. *Astrophys. J. Suppl. Ser.*, **27,** 21.
Phillips, M. M., Jenkins, C. R., Dopita, M. A., Sadler, E. M. & Binette, L. 1986. *Astr. J.*, **91,** 1062.
Pickles, A. J., 1985. *Astrophys. J.*, **296,** 340.
Raymond, J. C., 1979. *Astrophys. J. Suppl. Ser.*, **39,** 1.
Raymond, J. C. & Smith, B. W., 1977. *Astrophys. J. Suppl. Ser.*, **35,** 419.
Romanishin, W., 1985. *Astrophys. J.*, **289,** 570.
Rose, J. A., 1985. *Astr. J.*, **90,** 1927.
Rubin, V. C., Ford, W. K. Jr, Peterson, C. J. & Oort, J. H., 1977. *Astrophys. J.*, **211,** 693.
Sandage, A., 1971. In: *Study Week on Nuclei of Galaxies,* p. 271, ed. O'Connell, D. J. K., North-Holland, Amsterdam.
Sarazin, C. L., 1986. *Rev. mod. Phys.*, **58,** 1.
Sarazin, C. L. & O'Connell, R. W., 1983. *Astrophys. J.*, **268,** 552.
Seaton, M. J., 1979. *Mon. Not. R. astr. Soc.*, **187,** 75P.
Siegel, S., 1956. In: *Nonparametric Statistics,* p. 202, McGraw-Hill Kogakusha.
Smith, L. F., Biermann, P. & Mezger, P. G., 1978. *Astr. Astrophys.*, **66,** 65.
Stewart, G. C., Fabian, A. C., Jones, C. & Forman, W., 1984. *Astrophys. J.*, **285,** 1.
Thomas, P. A., Fabian, A. C., Arnaud, K. A., Forman, W. & Jones, C., 1986. *Mon. Not. R. astr. Soc.*, **222,** 655.
Tonry, J. & Davis, M., 1979. *Astr. J.*, **84,** 1511.

Note added in proof

We have noticed an error in the calculation of our Hβ line luminosities which has made them systematically too high by typically 10 per cent. Values of $L(\mathrm{H}\beta)$ and H_{rec} in Table 6 should all be divided by $(1+z)^2$. The changes to the ordinates in Figs 2, 3 and 6 will be imperceptible. Equations (8) and (9) are correct. These detailed changes do not affect the analysis, discussion or conclusions of this paper.